# Perspective on Integrated Photonic Devices using Transparent Conductive Oxides: Challenges and Opportunities

Alan X. Wang,<sup>1,\*</sup> and Wei-Che Hsu<sup>1,2</sup>

Abstract—Transparent conductive oxides (TCOs) are gaining increasingly high research interests for integrated photonic devices due to the strong plasma dispersion effect and process compatibility with versatile optoelectronic platforms. In this perspective article, the authors gave a brief review of research efforts both on theoretical modeling and experimental demonstration of integrated photonic devices, especially on highefficiency electro-optic modulators through the integration with plasmonics and silicon photonics. In addition, the authors discussed the challenge and opportunity associated with TCO photonic devices and the application in photonic integrated circuits (PICs) with emphasis on high mobility materials, highspeed E-O modulators, and large-scale integration. Finally, we conclude that collaboration with existing silicon photonics foundry is a necessary route to incorporate TCOs into existing PIC ecosystems.

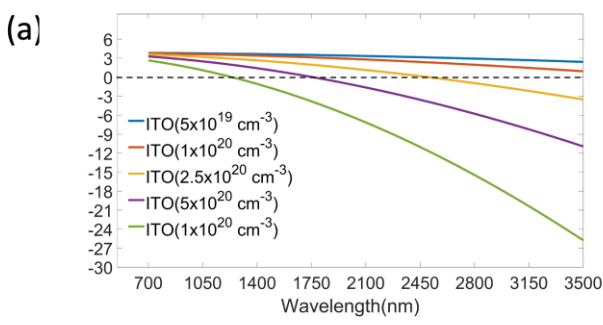
### I. INTRODUCTION

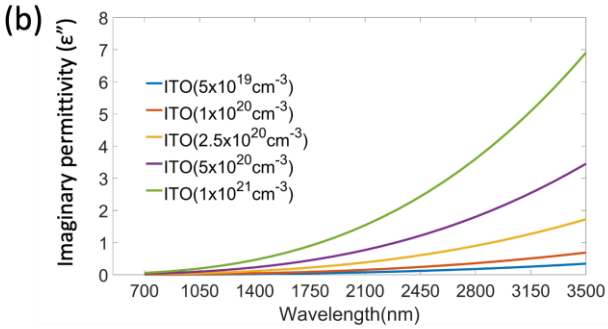
Transparent conductive oxides (TCOs) are typically doped metal oxides such as indium tin oxide (ITO) and aluminumdoped zinc oxide (AZO) that possess wide bandgap as well as high electrical conductivity. 1-4 The optical response of TCOs in the short wavelength range is governed by the fundamental band-to-band absorption (usually >3eV), which makes them highly transmissive in the visible spectral range. Coupled with their high electrical conductivity, TCOs are traditionally used as excellent electrode materials in flat panel displays and photovoltaics, which has fostered a large commercial market value of \$475.5M in 2022 with an expected compound annual growth rate (CAGR) of 16.9% from 2022 to 2028, according to Business Research Insights.<sup>5</sup> With contrastive optical properties in the long wavelength range (>1100nm), TCOs exhibit metallike behavior such as high reflection and plasmon absorption in the near-infrared (NIR) and mid-infrared (MIR) depending on the doping concentration, which is induced by collective oscillations of conduction band electrons known as plasma oscillations or plasmons for short. Windows with TCO coatings can reflect NIR and MIR efficiently in preventing radiative heat loss, 6 terming them "low-e" windows that are ideal for use in cold climates. Despite of these tremendously successful applications in traditional optical engineering, the potential of TCOs in integrated photonics was only realized in early 2010s as a plasmonic material that can offer extremely large refractive index modulation due to the free carrier effect. 7,8 Most TCOs are n-type degenerate semiconductors with high electron density coming from oxygen vacancies and addition of n-type dopants. The optical properties of TCOs in the long wavelength

range can be accurately described by the well-established Drude Model:<sup>9</sup>

$$\epsilon_r = \epsilon' + i\epsilon'' = \epsilon_{\infty} - \frac{\omega_p^2}{\omega^2 + v^2} + i \frac{\omega_p^2 \gamma}{\omega(\omega^2 + v^2)} \tag{1}$$

Here,  $\epsilon_{\infty}$  is the high-frequency dielectric constant.  $\omega_p$  is the plasma frequency, which is proportional to the carrier concentration  $N_c$  by  $\omega_p = \frac{N_c q^2}{\epsilon_0 m^*}$ , where q is the charge of the electron,  $\epsilon_0$  is the permittivity of vacuum, and  $m^*$  is the effective mass of the carrier. The plasma collision frequency  $\gamma$  is inversely proportional to the carrier mobility  $\mu$  by  $\gamma = \frac{m^*}{q u}$ . It





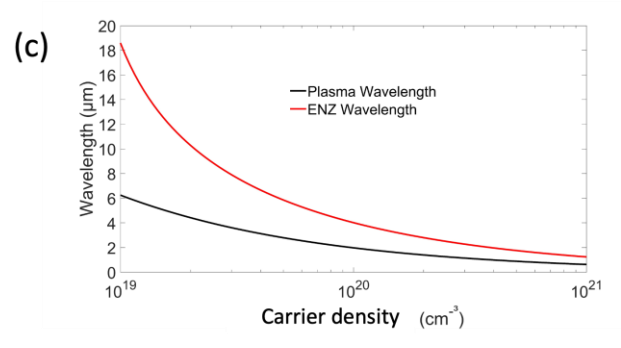


Fig. 1 Simulated (a) real permittivity and (b) imaginary permittivity of ITO with different carrier concentrations; and (c) simulated plasma wavelength and ENZ wavelength of ITO with carrier density from 10<sup>19</sup>/cm³ to 10<sup>21</sup>/cm³. Note: The simulation assumes a carrier mobility of 40 cm²V-¹s-¹.

<sup>&</sup>lt;sup>1</sup>Department of Electrical and Computer Engineering, Baylor University, One Bear Place #97356, Waco, Texas 76798, USA

<sup>&</sup>lt;sup>2</sup>School of Electrical Engineering and Computer Science, Oregon State University, Corvallis, Oregon 97331, USA

<sup>\*</sup>alan wang@baylor.edu

can be seen that the change of carrier concentration  $N_c$  always results in the change of both the real  $(\varepsilon')$  and imaginary  $(\varepsilon'')$ parts of the optical permittivity. Such carrier-induced optical properties of TCOs can be realized by two different approaches. The static approach seeks control of the oxygen vacancy or dopant density, which can tune the free carrier concentration  $N_c$ from the low 10<sup>19</sup>/cm<sup>3</sup> to well above 10<sup>21</sup>/cm<sup>3</sup> practically, which induces strong plasma dispersion effect to the optical permittivity. For example, Fig. 1(a) and (b) show the real and imaginary optical permittivity of ITO with different carrier from  $5 \times 10^{19} / \text{cm}^3$ to  $1 \times 20^{21}$ /cm<sup>3</sup>. concentrations Correspondingly, the plasma wavelength is shifted from 6µm to 0.8 µm, as shown in Fig. 1 (c). Of particular interests to TCO materials are epsilon-near-zero (ENZ) effects when the real permittivity  $\varepsilon$ ' is zero and the imaginary permittivity  $\varepsilon$ " is very small, resulting in absolute |E| close to zero. The ENZ wavelength of ITO versus the carrier concentration is also shown in Fig. 1 (c), which sweeps through the entire MIR and NIR wavelength range. In recent years, extremely strong nonlinear optical effect associated with hot electrons of ITO at the ENZ wavelength have been discovered10, and potential devices for all-optical-switching (AOS) were proposed and demonstrated. 11-13 TCO-based AOS devices can be developed by utilizing the thermal broadening of the Fermi-Dirac distribution, a consequence of electron plasma heating through pulsed pump-probe configurations. This approach promises sub-picosecond, femtojoule-level AOS devices remarkable optical interaction, which is crucial for advancing technologies like spiking neural networks. Nevertheless, the static approach is constrained by that the carrier density is deterministic upon the sputtering deposition and cannot be altered in a practical manner for many optoelectronic devices.

A more desirable approach is based on dynamic modulation of free carriers through electrical gating using a metal-oxidesemiconductor capacitor (MOSCAP) structure. The gate voltage induces either accumulation or depletion of electrons in the TCO material and provides an efficient and rapid electrooptic (E-O) modulation of the effective index to the waveguide mode. Various MOSCAP devices have been experimentally demonstrated. Depending on the functionality of the TCO material, we summarize the schematic of these devices in Fig. 2 (a-d): a) metal (usually Au) as the gate and bulk TCO as the semiconductor waveguide;14,15 b) metal as the gate and TCO thin film on bulk silicon (Si) as the semiconductor waveguide; 16,17 c) metal and TCO thin film as the gate and ptype silicon (p-Si) as the semiconductor waveguide; 18,19 and d) TCO as the gate and p-Si as the semiconductor waveguide. <sup>20,21</sup> Each configuration offers unique advantages for integrated photonic devices but is also subject to certain limitation as briefly summarized here. In MOSCAP (a) and (b), the E-O modulation only comes from accumulated electrons in the TCO layer since holes in the metal layer play negligible roles. In MOSCAP (c) and (d), the E-O modulation comes from both accumulated electrons in the TCO and holes in the p-Si layer, which will induce a stronger plasma-dispersion effect. In addition, MOSCAP-(a) provides extremely compact mode volume due to the plasmonic slot waveguide and can offer large E-O modulation efficiency with the price of large optical waveguide loss. For MOSCAP-(b) and (c), they can slightly lower the waveguide loss, but the E-O modulation efficiency is also comprised as the mode profile is less confined. MOSCAP-(d) achieves the lowest waveguide loss since there is no plasmonic structure involved. However, the optical mode is least confined, and the effective index modulation is relatively moderate.

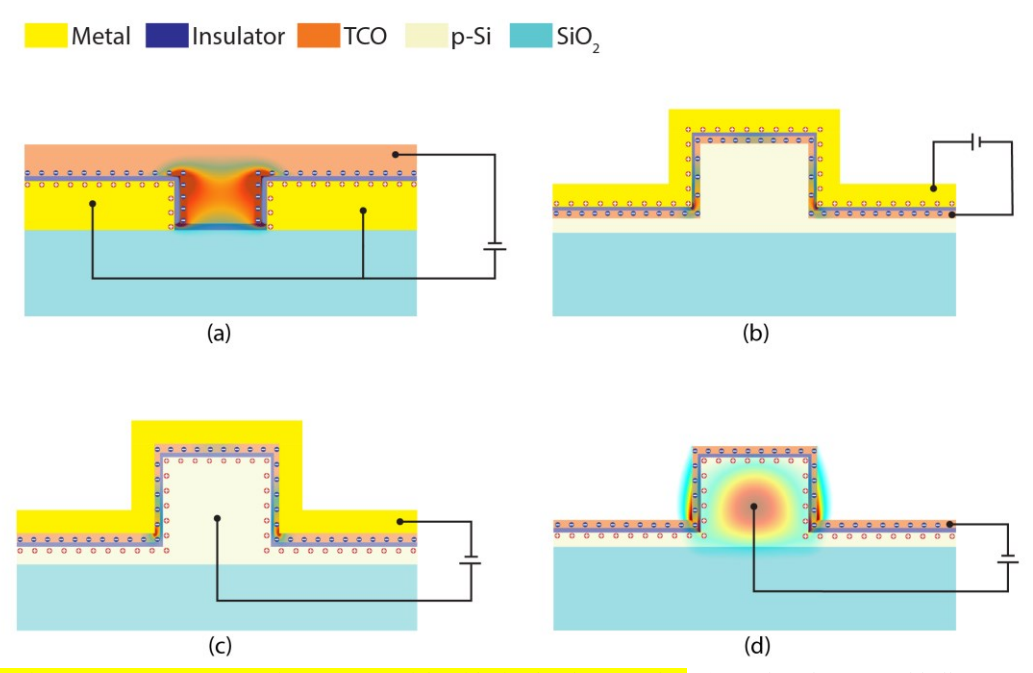


Fig. 2 Schematic of various MOSCAP structures using TCO materials with simulated TE<sub>0</sub> modes: (a) metal as the gate and bulk TCO as the semiconductor waveguide; b) metal as the gate and TCO thin film on bulk Si as the semiconductor waveguide; c) metal and TCO thin film as the gate and p-type silicon (p-Si) as the semiconductor waveguide; and d) TCO as the gate and p-Si as the semiconductor waveguide.

### II. REVIEW OF HISTORY

The development of TCO-based integrated photonic devices started from the search of better plasmonic materials with large refractive index tunability.<sup>22,23</sup> Compared with traditional plasmonic materials such as noble metals ( $N_c \sim 5 \times 10^{22} / \text{cm}^3$ ) and transitional metal nitrides ( $N_c \sim 1 \times 10^{22}$ /cm<sup>3</sup>), TCO has a desired  $N_c$  around  $10^{20}$ /cm<sup>3</sup> and can bridge the gap with traditional degenerate semiconductors ( $N_c \sim 1 \times 10^{19} \text{cm}^3$ ). In addition, the  $N_c$ of TCOs can be dynamically tuned by almost two orders of magnitude (10<sup>19</sup>~10<sup>21</sup>/cm<sup>3</sup>) through electrical gating, resulting in large tunability of the ENZ wavelength across the NIR and MIR range as shown in Fig. 1 (c). Since then, many integrated photonic devices using TCOs14-21 have been demonstrated, especially with the focus on electro-absorption (EA) modulators induced by the ENZ effect. Several comprehensive review articles about TCO modulators<sup>24-26</sup> and ENZ photonics using TCO materials<sup>27-29</sup> have been published in the past years. The intention of the brief review in this perspective article is not to repeat previous work. Instead, we would focus on summarizing previous research of TCO-based integrated photonic devices from four different perspective angles that are critical for future research and development.

## A. Modeling of charge accumulation

Three different models have been investigated to treat the charge accumulation under the gate bias as shown in Fig. 3. First, the uniform concentration model simplifies the

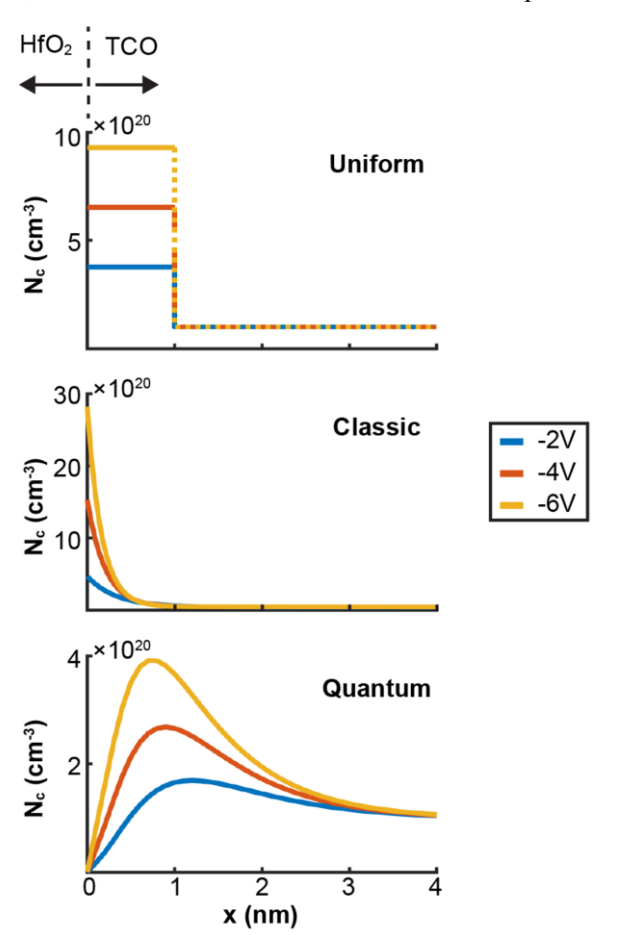


Fig. 3 Comparison of accumulated charge distribution in the TCO layer using uniform distribution model, classic model, and quantum moment model.

accumulated charges as a thin layer of electron gas with uniform density. The problem with this simple model is that the thickness of the accumulation layer was arbitrary in early years, varying from sub-nanometers to tens of nanometers in different literatures. 30-36 Since the capacitance density of the MOSCAP is mainly determined by the gate insulator thickness and dielectric constant, arbitrary assumption of the accumulation layer thickness will result in a big difference of the carrier density, and hence large variation of the driving voltage and EA efficiency at the ENZ wavelength. For instance, a 0.5nm accumulation layer can be easily switched to ENZ as the calculated carrier density is large while the EA strength will be relatively weak. As a comparison, a 5nm accumulation layer will induce unrealistically strong EA strength (>10dB/μm), but it requires a very large electric field that can cause breakdown of the insulation layer. The second approach, classic model, calculates the carrier distribution as a stationary solution. 37-39 From the simulation results, the maximum carrier density occurs at the TCO-insulator interface and decays exponentially with a steep slope. The EA strength calculated by the classic model is generally lower than that obtained by uniform concentration model since the classic model gives a very steep profile slope of the free carrier distribution, and the effective ENZ layer is much thinner. More significantly, as shown by U. Koch et al.,37 the classic model predicts a digital transfer function with two well-defined ON-and-OFF states. In other words, the maximum EA will saturate as the driving voltage reaches the value for ENZ. As a comparison, uniform concentration model presents strongly enhanced EA strength at the ENZ voltage like a resonator, which is caused by the field enhancement in the uniform layer. However, neither the digital transfer function nor the resonator-like feature has been experimentally observed. Our group applied the quantum moment model, as the third approach, to analyze the free carrier distribution of the TCO-driven MOSCAP and revealed significantly different device physics compared with previous simulation models. 40,41 The quantum moment model predicts the pin-down of the carrier concentration at the interface and several angstroms shift of the peak concentration into the semiconductor layer. The shift of the charge maximum effectively increases the thickness of the insulating layer as the centroid of the charges in TCO and silicon are separated further away from each, which decreases the capacitance of the MOS capacitor. In addition, the charge distribution of the quantum model is much wider than that predicted by the classic model. As results, the quantum moment model points out a much higher driving voltage to turn the TCO materials into ENZ and a stronger modulation strength compared with the classic model. Through comparison with experimental results, we proved that the quantum model has a better match in terms of the EA strength and the driving voltage. The quantum moment model was also applied to study MOSCAP-driven silicon waveguides with various semiconductor gate materials, and the E-O modulation efficiency was compared. 41 Note: the classic and quantum moment models were simulated using commercial semiconductor simulation software Silvaco. For 1-D carrier distribution, it might be possible to develop a simple analytical

model based on machine-learning analysis of the numerical simulation results.

We must point out that the difference between these three models is significant only when we design ENZ photonic devices. For regular refractive index modulation from the plasma dispersion effect in which the change of  $N_c$  in the accumulation layer is moderate, and the TCO is far from the ENZ condition, the total amount of accumulated charges weighs much more than the distribution of these charges. Our simulation results show very little difference in the effective index modulation. In such cases, using a 1 to 2 nm uniform layer can greatly simplify the analysis with acceptable accuracy.

## B. EA modulators using the ENZ effect

Compared with traditional degenerate semiconductors such as heavily doped Si and GaAs that show ENZ behaviors at the MIR range, TCOs can be switched to ENZ at the NIR wavelength due to two unique features. First, the high frequency permittivity  $\epsilon_{\infty}$  of TCOs is around 4, which is much lower than that of Si or III-V semiconductors with values above 12. Second, the spreading of accumulated electrons or holes in the accumulation layer is determined by Debye length:

$$L_D = \sqrt{\frac{\epsilon k_B T}{q^2 N_C}} \tag{2}$$

where  $k_B$  is the Boltzmann's constant, T is the absolute temperature in kelvins, and q is the charge of the electron. Because of the low dielectric constant  $\epsilon$  and high background doping concentration  $N_c$ , the Debye length of TCO is much smaller than that of Si or GaAs, resulting in much higher carrier density in the thinner accumulation layer. Therefore, a moderate gate bias can induce accumulation of free carriers above 6.5×10<sup>20</sup> cm<sup>-3</sup>, causing the real permittivity of TCOs to reach zero while the absolute permittivity is a minimum value due to the small value of the imaginary part. Such property has enabled near-zero refractive index photonics 27,29,42-44 — the study of light-matter interactions in the presence of structures with near-zero parameters, either the relative optical permittivity or permeability. ENZ photonics exhibits a number of unique features including decoupling of their spatial and temporal field variations, tunneling through arbitrary channels, constant phase transmission, strong field confinement, and ultrafast phase transitions. Compared with traditional dielectric or metallic photonic materials, ENZ photonics not only enables unprecedented electromagnetic wave dynamics and lightmatter interactions, but also paved the road toward a new generation of photonic devices such as directed light emission devices, 45,46 nonlinear optical devices, 10,47 harmonic frequency conversion, 48,49 electro-absorption 15,16,18,19 modulation<sup>50</sup> — just to name a few.

So far EA modulators induced by the ENZ effect are the mostly exploited TCO photonic devices. These EA modulators can achieve strong modulation strength of 1~3dB/μm, which were summarized in our previous article.<sup>40</sup> Such strong EA strength comes from two physics mechanisms. First, the electric field polarized perpendicular to the accumulation layer

will be strongly enhanced in the ENZ layer due to the continuity of electric field displacement, resulting in concentration of the optical mode to a few nanometers scale. <sup>51,52</sup> Second, the optical absorption of TCO materials is determined by

$$\alpha = \frac{Im(\varepsilon)}{|\varepsilon|^2} \tag{3}$$

At the ENZ wavelength, the real part of  $\epsilon$ ' is zero, and the absolute value  $|\epsilon|$  is equal to the imaginary part  $|\epsilon$ '', therefore the ENZ absorption is given by

$$\alpha = \frac{1}{Im(\varepsilon)} = \frac{1}{|\varepsilon''|} \tag{4}$$

Equation (4) indicates a very large EA strength since  $|\varepsilon|$  is generally quite small. It is counter-intuitive that at the ENZ condition, a smaller imaginary permittivity induces larger optical absorption. While under a normal condition, a larger imaginary permittivity means higher optical loss.

## C. Non-ENZ photonic devices: resonators and phase tuners

Compared with plasmonic and ENZ photonic devices, using TCOs as regular semiconductor materials for optical resonators and phase tuners with moderate refractive index modulation has received much less attention. However, such non-ENZ TCO photonic devices might be more practical for integrated photonic devices and large-scale PICs. First, it does not require the integration with plasmonic materials to enhance the optical field concentration, and thus it will greatly reduce the optical waveguide loss. This is a very crucial requirement when using cascaded photonic devices for complex information processing. Second, non-ENZ devices can be driven by a much smaller gate voltage compared with ENZ photonic devices, which will reduce the energy consumption and minimize the challenge to high-speed E-O modulation. Third, the relatively low driving voltage eases the concern of breakdown of the insulator layer and increases long-term reliability. Last but not least, non-ENZ photonic devices only require a simple sputtering process of TCO materials and can be more easily integrated with silicon photonics, which is the most crucial platform for large-scale PICs.

Two types of TCO-driven resonators, photonic crystal (PC) nanocavity modulators<sup>20,53,54</sup> and microring resonators (MRRs)<sup>21,55-57</sup>, have been reported by our group. The E-O efficiency of optical resonators is typically expressed as the peak wavelength shift divided by the driving voltage with a unit of picometer per volt (pm/V). The E-O efficiency is determined by the plasma-dispersion effect of semiconductor materials, the capacitance density of the device, and the overlapping factor between accumulated charges and optical modes. Typically, TCO-driven optical resonators use a thin layer of high dielectric constant insulator such as hafnium oxide (HfO<sub>2</sub>) to improve the E-O efficiency. For example, the PC nanocavity modulator with 10nm HfO<sub>2</sub> achieved an E-O efficiency of 250pm/V,<sup>53</sup> while the MRR with 9nm HfO<sub>2</sub> and narrowed waveguide with a large overlapping factor demonstrated an unprecedented record of 589 pm/V.<sup>57</sup> Detailed analysis of TCO-based resonator

modulators, as well as the comparison between MOSCAP and reversed PN junction devices can be found in our previous article. So We need to point out that from our theoretical study, So TCOs are not the most E-O efficient gate materials for MOSCAP devices since graphene and some III-V compound semiconductors can provide even larger E-O modulation effect. However, TCOs demonstrated the best experimental results, which is possibly due to the easy integration with silicon photonics that can conformally cover the silicon waveguide to achieve better overlapping factors.

Although MRRs are intrinsically based on phase tuning, phase tuners we discussed here only refer to phase modulators and Mach-Zehnder interferometer (MZI) modulators. Currently, only MZI modulators using ITO have also been reported with a very low half-wave voltage and length product  $(V_{\pi} \cdot L)$  of 0.52 V·mm. <sup>17,50</sup> The active modulation length is 30 $\mu$ m with a driving voltage of 12V, which is still away from the ENZ condition. What seems to be a limiting factor to achieve lower driving voltage is the optical loss, which makes a long active device length undesirable as we pointed out in our modeling. <sup>41</sup>

# D. High mobility TCO materials

High mobility transparent conductive oxides (HMTCOs) will benefit both ENZ and non-ENZ optical modulators. From Drude model, a larger carrier mobility will reduce the plasma collision frequency y, and hence suppress the imaginary part of the optical permittivity. Table I compared several typical TCO materials in terms of carrier density, carrier mobility, absolute value of the permittivity  $|\varepsilon|$  at the ENZ wavelength, effective mass, and optical loss at 1550nm wavelength when the carrier density is 10<sup>20</sup>cm<sup>-3</sup>. For EA modulators based on the ENZ effect, the extinction ratio (ER) is inversely proportional to the absolute value of the permittivity  $|\varepsilon|$  at the ENZ wavelength. It has been suggested that CdO with a high mobility of 300 cm<sup>2</sup>V<sup>-</sup> <sup>1</sup>s<sup>-1</sup> can potentially reach an ER over 5dB/µm.<sup>30</sup> The dependence of driving voltage and energy efficiency on the mobility of various TCO materials was simulated and compared by our previous work.64

For non-ENZ devices such as MRRs, as illustrated in Fig. 4 (a), using HMTCO as the MOSCAP gate material will bring unrivaled advantages because it will lower the optical

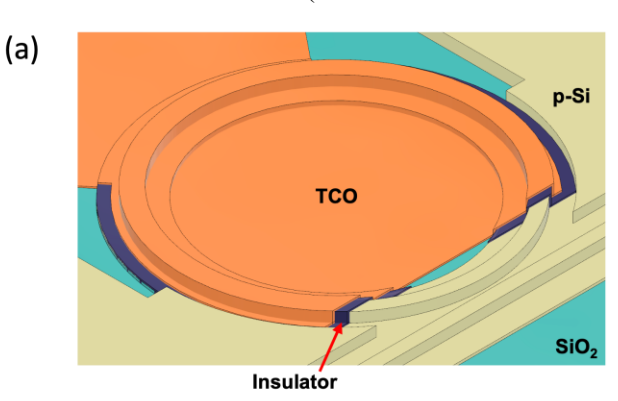
TABLE I

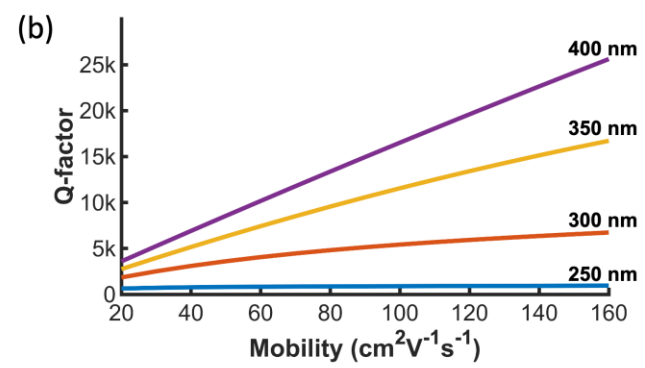
COMPARISON OF TYPICAL TCO MATERIALS AS CANDIDATES FOR MOSCAP
INTEGRATED PHOTONIC DEVICES

| INTEGRATED THOTONIC DEVICES |                              |   |           |      |   |  |  |  |  |  |  |
|-----------------------------|------------------------------|---|-----------|------|---|--|--|--|--|--|--|
| TCOs                        | Carrier density (1/cm³)      | Carrier<br>mobility<br>(cm <sup>2</sup> V <sup>-1</sup> s <sup>-1</sup> ) | ENZ<br> ε | m*   | Optical loss @1550nm with $N_c=1\times10^{20}/cm^3$ (dB/ $\mu$ m) |  |  |  |  |  |  |
| ITO <sup>59</sup>           | $10^{19}\!\!\sim\!\!10^{21}$ | 15~30   | 0.96      | 0.35 | 0.050   |  |  |  |  |  |  |
| $In_2O_3^{60,61}$           | $10^{18}\!\!\sim\!\!10^{20}$ | 20~35   | 0.42      | 0.32 | 0.046   |  |  |  |  |  |  |
| $ITiO^{62}$                 | $10^{20}\!\!\sim\!\!10^{21}$ | 60~90   | 0.15      | 0.31 | 0.020   |  |  |  |  |  |  |
| $IHO^{61}$                  | $10^{20}$                    | 120~150   | 0.10      | 0.27 | 0.015   |  |  |  |  |  |  |
| CdO <sup>63</sup>           | $10^{19}\!\!\sim\!\!10^{20}$ | 280~300   | 0.05      | 0.22 | 0.011   |  |  |  |  |  |  |

ITO: Indium-tin oxide, In<sub>2</sub>O<sub>3</sub>: Indium oxide, ITiO: Titanium-doped indium oxide, IHO: Hydrogen-doped indium oxide, CdO: Cadmium oxide.

waveguide absorption and hence improves the Q-factor of the MRR as shown in Fig. 4 (b), which simulated the TCO-gated silicon MRRs with different waveguide widths. In addition, high carrier mobility usually results from smaller effective mass of conduction band electrons and therefore, HMTCO will induce stronger plasma dispersion effect and larger E-O modulation efficiency according to Drude model. When experimentally comparing the performance of ITO-gated and ITiO-gated MRRs with nearly identical waveguide geometry, the advantages of employing HMTCO as the gate material become more pronounced. The ITO-gated MRR,<sup>21</sup> with lower carrier mobility, exhibited a Q-factor of approximately 1500 and an E-O efficiency of 271 pm/V. In contrast, the ITiO-gated MRR,<sup>57</sup> featuring the same waveguide width but higher carrier mobility, demonstrated an improved Q-factor of 5200 and a higher E-O efficiency of 589 pm/V. Notably, both devices utilized different thicknesses (16 nm for the ITO device and 9





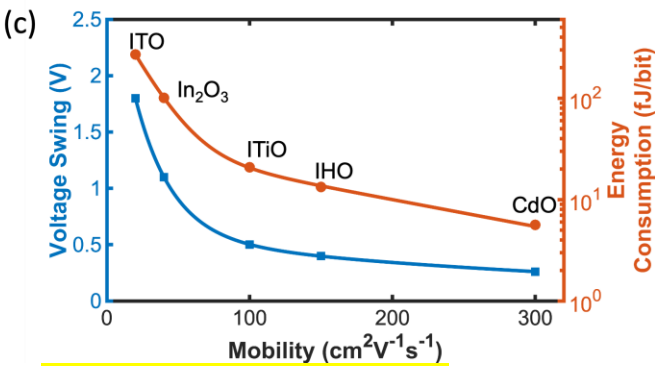


Fig. 4 (a) 3D schematic of a TCO-gated silicon MRR. (b) Simulated Q-factor of MRRs versus the carrier mobility for various microring waveguide widths. (c) Simulated driving voltage and energy consumption of MRMs driven by different TCO materials. Note: Simulation results are based on a ring radius of 8um.

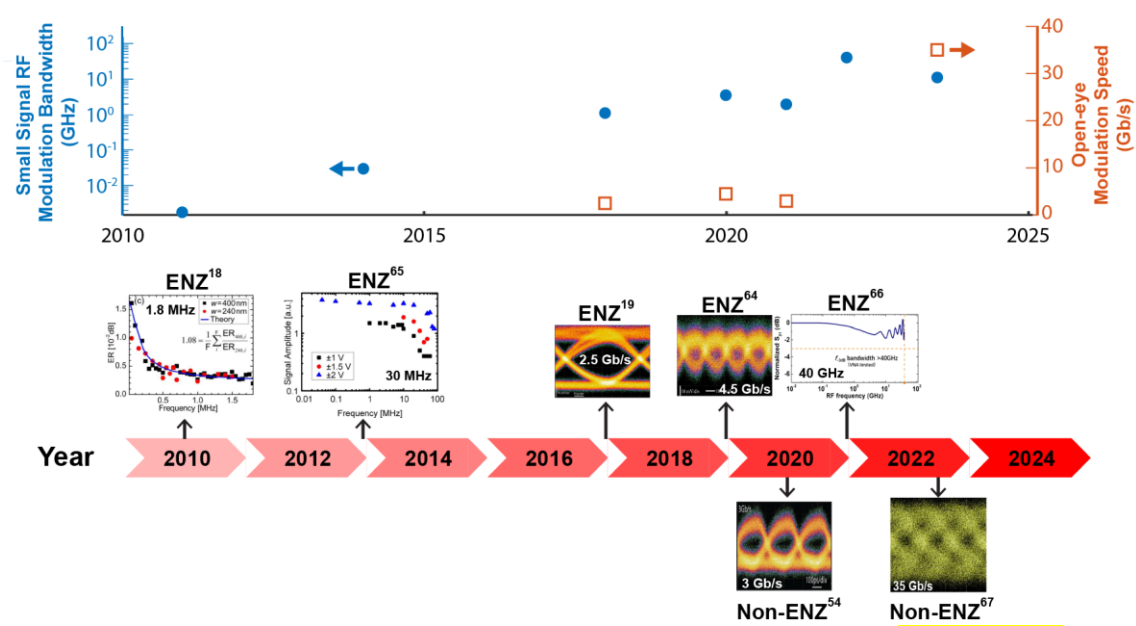


Fig. 5 Timeline of MOSCAP high-speed modulators with TCO gates. We only included experimental results of either frequency response or eye diagrams above 1Gb/s.

nm for the ITiO device), which can influence E-O efficiency because E-O efficiency is linearly proportional to capacitance density. Even when assuming equal HfO<sub>2</sub> thickness in both devices, the ITiO-gated MRR still exhibited higher E-O efficiency. This comparison underscores the improved Q-factor and higher E-O efficiency from using HMTCO as the gate material. Because of the improved Q-factor and higher E-O efficiency, HMTCO will lower the driving voltage and reduce the energy consumption of microring modulators (MRMs), as illustrated in Fig. 4 (c). It shows that HMTCO can potentially reduce the driving voltage to 0.5V and energy consumption below 1fJ/bit. From the bandwidth perspective, the high conductivity from HMTCOs will reduce the series resistance and hence improve the RC-delay limited bandwidth as well.

### E. The Holy Grail: High-speed and large-scale integration

Since the first experimental demonstration of TCO devices in 2010,<sup>7,8</sup> high-speed E-O modulation has remained a grand challenge due to both fundamental problems related to TCO

materials and engineering issues for high-speed design. First, the carrier density and mobility of TCO materials strongly depend on the sputtering deposition and post-processing conditions. As results, such complexity presents difficulties in assessing the consistency of carrier mobility across different materials and thicknesses. Our previous work showed that the leakage current density versus the gate voltage, and the capacitance density versus the frequency can be strongly affected by the conductivity of ITO.64 Low conductivity ITO showed very sluggish frequency response and demonstrated much lower bandwidth predicted by the RC-delay limit, which suggested more complex mechanisms such as surface-trapped charges in the MOSCAP due to the ITO/HfO2 interface. Second, achieving high-speed E-O modulation requires sophisticated doping to both silicon and TCO to reduce the series resistance, optimization of the fabrication process to form good Ohmic contact, and precise design of high-speed electrodes for impedance matching. Especially, TCO materials seem to be quite picky to metal films that can form Ohmic

| TABLE II   |
|--|
| COMPARISON OF HIGH-SPEED TCO-DRIVEN E-O MODULATORS |

| COMPARISON OF HIGH-SPEED TCO-DRIVEN E-O MODULATORS |           |                |            |            |                                 |                     |                             |     |  |  |
|--|-----------|----------------|------------|------------|---------------------------------|---------------------|-----------------------------|-----|--|--|
| Modulator<br>structure                             | TCO       | $V_{pp} \ (V)$ | IL<br>(dB) | ER<br>(dB) | E-O bandwidth $(f_{3dB})$ (GHz) | Data rate<br>(Gb/s) | Energy consumption (fJ/bit) | Ref |  |  |
| ENZ  | $In_2O_3$ | 2              | 10         | 6.5        | 1.1                             | 2.5                 | 2100                        | 19  |  |  |
| ENZ  | ITO       | 20             | 6.7        | ~2.5       | 1.1                             | -                   | 2046                        | 17  |  |  |
| ENZ  | ITO       | 2              | 21.6       | 3.2        | 3.5                             | 4.5                 | 64                          | 64  |  |  |
| ENZ  | $In_2O_3$ | 12             | 4.5        | 1.4        | >40                             | -                   | 234                         | 66  |  |  |
| ENZ  | ITO       | 5              | 8.6        | <1.8       | >40                             | -                   | -                           | 68  |  |  |
| Non-ENZ<br>(PC cavity)                             | ITO       | 2              | 7.8        | 3.45       | 1.94                            | 3                   | 18.3                        | 54  |  |  |
| Non-ENZ<br>(MRR)                                   | ITiO      | 0.8            | 3          | 6          | 11                              | 25                  | 53                          | 67  |  |  |

<sup>-:</sup> Did not mention in the article.

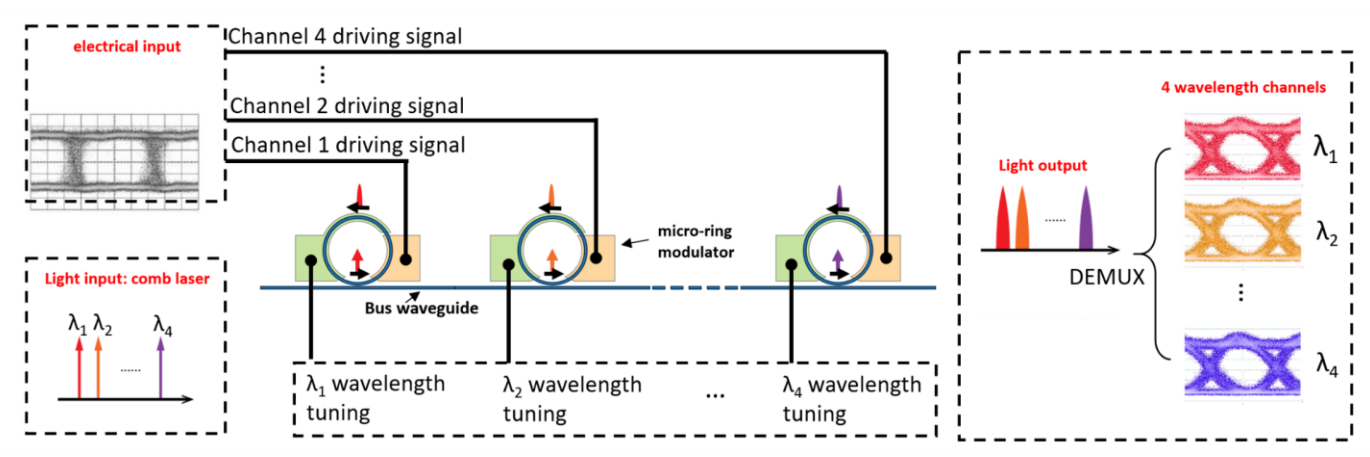


Fig. 6 A proposed 4-channel on-chip WDM transmitter that can perform E-O modulation and wavelength MUX/DeMUX independently.

contact with small contact resistance. According to our experiences, a metal film consists of 5nm nickel and 100nm gold is a good choice, while a typical aluminum film does not work. Another pain point is that no silicon photonics foundry is offering TCO processes in the fabrication and many experimental groups haveto rely on their own facilities to complete the entire fabrication steps. Researchers in TCO photonics are facing issues such as waveguide loss, coupling loss, doping of silicon, and control of the working wavelength, just like those to silicon photonics in early years.

Nevertheless, several groups have demonstrated high-speed E-O modulators using TCOs. Fig. 5 illustrates the progression of bandwidth performance over time, indicating a growing interest and experimental achievements in higher bandwidth capabilities in TCO-driven E-O modulators. Additionally, Table II summarizes experimental results related to high-speed TCO-driven E-O modulators. In recent years, TCO-driven E-O modulators utilizing ENZ structures have achieved bandwidths exceeding 40 GHz, but only with small RF signal modulation. <sup>66,68</sup> No open eyes of E-O modulated signals were observed. Such high bandwidth is attributed to the direct placement of an Au electrode on the active region, which significantly reduces series resistance and enhances bandwidth. However, it comes with trade-offs of increased insertion loss, higher driving voltage, and compromises in the extinction ratio. On the other hand, TCO-driven E-O modulators based on non-ENZ structures have also seen significant progress, aiming to address the drawbacks associated with ENZ structures. Experimental data have showcased bandwidths exceeding 11GHz, with the potential for further improvements to 52GHz through optimized fabrication processes.<sup>67</sup> Most importantly, clear and open eyes at high speed of more than 25Gb/s were experimentally obtained with sub-volt driving voltage, demonstrating enormous potentials for optical communication computation. Overall, the continuous evolution of TCO-driven E-O modulators with both ENZ and non-ENZ structures has paved the way for higher-speed data transmission with low driving voltage and high energy efficiency.

To achieve large-scale integration, implementing wavelength division multiplexing (WDM) via cascaded MRR arrays driven by HMTCO offers a solution to overcome the significant challenge of precise wavelength control while minimizing

power consumption compared to traditional WDMs.<sup>57</sup> Taking the advantage of HMTCO, MRRs within the WDM not only achieve higher Q-factors but also exhibit remarkable E-O efficiency, enabling a broad wavelength tuning range with low voltage and power requirements. Additionally, gate biases can be utilized to compensate for resonant wavelength shifts in the MRRs resulting from fabrication discrepancies or temperature fluctuations.<sup>56,57</sup> In this configuration, each MRR within the WDM can be independently tuned by applying gate bias, allowing for precise channel spacing control and ensuring uniformity across the WDM system. This approach represents a promising advancement in large-scale integrated optical networks, offering enhanced performance and addressing power consumption concerns.

This pioneering work laid a foundation for future on-chip optical interconnects with high bandwidth density. Fig. 6 proposes an on-chip WDM transmitter consisting of a silicon bus waveguide coupled to multiple dual-functional TCO-driven MRMs, which will be driven by two independent electrodes: a wavelength tuning electrode will be driven by low-speed, large DC voltage or slow-varying signals, and an E-O modulation electrode receives high-speed, small voltage RF or digital signals for efficient EO conversion. Four constant-wave (CW) lasers with wavelengths of  $\lambda_1$  to  $\lambda_N$  (N=4, 8, ...) in the figure are coupled into the bus waveguide, and each microring resonator can perform high-speed E-O modulation and wavelength multiplexing/de-multiplexing (MUX/DeMUX) independently. In the meanwhile, these MRMs with dual electrodes can adjust its own working wavelength over a large range to dynamically compensate for fabrication errors and temperature variation. Since there is almost no electric current flowing through the gate insulator, we can achieve near-zero static power consumption for wavelength tuning, which eliminates power-hungry thermal heaters that have been widely used in silicon PICs.

### III. OUTLOOK AND CONCLUSIONS

Significant research and development efforts are still needed to improve the bandwidth of TCO-driven E-O modulators above 50GHz and achieve clear-eye modulation at 100Gb/s and above to meet state-of-the-art optical communication

requirement. The driving voltage further down to 0.5V is necessary for energy-efficient operation. Of all existing optoelectronic platforms, integrating TCOs with silicon photonics is the most promising approach to leverage the matured fabrication process for large-scale PICs with the benefit of enhanced E-O modulation performance. However, current silicon photonics foundry limits the process of silicon modulators to reversed PN junctions. Neither MOSCAP structures nor heterogeneously integrations with other functional materials are offered in existing fabrication shuttles. A feasible approach to solve this dilemma in the near future is to combine the silicon photonics shuttle with TCO patterning processes in each group. For example, we have explored the fabrication process of Si-TCO MOSCAP modulators by combining Intel's silicon photonics fab with our own TCO patterning process. <sup>67</sup> Specifically, we used Intel's 300 mm high volume manufacturing (HVM) silicon photonics process to fabricate passive Si-MRRs with p+ and p++ doping. After that, we continued the fabrication in our cleanroom to grow HfO2 as the insulator and pattern ITiO gates on Si-MRRs, with Ohmic contacts formed by Ni/Au electrodes. Our pioneering work demonstrated sub-volt, 35Gb/s MOSCAP Si-MRMs driven by ITiO gates. The advantages of such relayed fabrication include: 1) foundry offers high quality silicon waveguide layer with low optical loss, high fiber coupling efficiency, small deviation of resonant wavelengths, precise control of the doping profile, and the possibility of large-scale integration on centimeter-scale wafers; 2) foundry offers a large quantity of silicon photonics chips at relatively low cost so our group can focus on the most crucial fabrication processes to integrate TCO materials onto silicon photonic devices; and 3) the success of combined foundry-university co-fabrication will prove the feasibility of integrating TCO processes into silicon photonics foundry to achieve high-performance hybrid devices and PICs. Due to the versatile RF-sputtering process, TCOs can be deposited on various platforms that are not limited to silicon and plasmonic waveguides. One remarkable progress is the demonstration of E-O modulation on dielectric Si<sub>3</sub>N<sub>4</sub> using In<sub>2</sub>O<sub>3</sub>, which expanded the operational wavelength to 980nm wavelength since Si<sub>3</sub>N<sub>4</sub> is transparent in the NIR window.<sup>69</sup> However, it also poses a grand challenge to push the ENZ wavelength down to 980 nm, which requires extremely heavy doping and high driving voltage.

In conclusion, TCOs have attracted increasing research interests in recent years due to the extraordinary refractive index modulation and excellent process compatibility with existing PIC platforms. The application of TCO-driven modulators and PICs can go beyond traditional optical communications. The low driving voltage, high energy efficiency, and large wavelength tunability will make them uniquely suited for neuromorphic computing, artificial intelligence, optical phased array, as well as RF photonics. In our opinion, incorporating TCOs into existing photonics foundries will be the key factor to enable them in such system-level applications.

### **ACKNOWLEDGMENTS**

The authors acknowledge the financial support by the Intel URC project 76084461, the NSF GOALI project 2240352, the AFOSR MURI project FA9550-17-1-0071, and the NASA ESI program 80NSSC23K0195.

### **AUTHOR DECLARATIONS**

Conflict of Interest

The author has no conflict of interest to declare.

Data Availability

The data that support the findings of this study are available from the corresponding author upon reasonable request.

#### REFERENCES

- <sup>1</sup> G. V. Naik, V.M. Shalaev, and A. Boltasseva, "Alternative plasmonic materials: Beyond gold and silver," Adv. Mater. **25**(24), 3264–3294 (2013).
- <sup>2</sup> D.S. Ginley, and J.D. Perkins, in *Handb. Transparent Conduct.*, edited by D.S. Ginley (Springer US, Boston, MA, 2011), pp. 1–25.
- <sup>3</sup> K. Ellmer, "Past achievements and future challenges in the development of optically transparent electrodes," Nat. Photonics **6**(12), 809–817 (2012).
- <sup>4</sup> S. Calnan, and A.N. Tiwari, "High mobility transparent conducting oxides for thin film solar cells," Thin Solid Films **518**(7), 1839–1849 (2010).
- <sup>5</sup> Business Research Insights, "Transparent Conducting Oxide (TCO) Glass Market Size, Share, Growth, And Industry Analysis By Type (ITO Coated Glass, FTO Coated Glass, AZO Coated Glass) By Application (Flat Panel Display, Solar Battery & Others) Regional Forecast From 2022 To 2028," (2023). Available: <a href="https://www.businessresearchinsights.com/market-reports/transparent-conducting-oxide-tco-glass-market-103811">https://www.businessresearchinsights.com/market-reports/transparent-conducting-oxide-tco-glass-market-103811</a>.
- <sup>6</sup> J. Karlsson, and A. Roos, "Annual energy window performance vs. glazing thermal emittance the relevance of very low emittance values," Thin Solid Films **392**(2), 345–348 (2001).
- <sup>7</sup> A. Melikyan, T. Vallaitis, N. Lindenmann, T. Schimmel, W. Freude, and J. Leuthold, in *Conf. Lasers Electro-Optics 2010* (Optica Publishing Group, 2010), p. JThE77.
- <sup>8</sup> E. Feigenbaum, K. Diest, and H.A. Atwater, "Unity-order index change in transparent conducting oxides at visible frequencies," Nano Lett. **10**(6), 2111–2116 (2010).
- <sup>9</sup> P. Drude, "Zur Elektronentheorie der Metalle," Ann. Phys. **306**(3), 566–613 (1900).
- <sup>10</sup> M.Z. Alam, I. De Leon, and R.W. Boyd, "Large optical nonlinearity of indium tin oxide in its epsilon-near-zero region.," Science **352**(6287), 795–797 (2016).
- <sup>11</sup> E. Li, and A.X. Wang, "Femto-Joule All-Optical Switching Using Epsilon-Near-Zero High-Mobility Conductive Oxide," IEEE J. Sel. Top. Quantum Electron. **27**(2), 1–9 (2021).
- <sup>12</sup> J. Bohn, T.S. Luk, C. Tollerton, S.W. Hutchings, I. Brener, S. Horsley, W.L. Barnes, and E. Hendry, "All-optical switching of an epsilon-near-zero plasmon resonance in indium tin oxide.," Nat. Commun. **12**(1), 1017 (2021).
- <sup>13</sup> S. Saha, B.T. Diroll, J. Shank, Z. Kudyshev, A. Dutta, S.N. Chowdhury, T.S. Luk, S. Campione, R.D. Schaller, V.M. Shalaev, A. Boltasseva, and M.G. Wood, "Broadband, High-Speed, and Large-Amplitude Dynamic Optical Switching with Yttrium-Doped Cadmium Oxide," Adv. Funct. Mater. 30(7), 1908377 (2020).
- <sup>14</sup> H.W. Lee, G. Papadakis, S.P. Burgos, K. Chander, A. Kriesch, R. Pala, U. Peschel, and H.A. Atwater, "Nanoscale conducting oxide PlasMOStor," Nano Lett. **14**(11), 6463–6468 (2014).
- <sup>15</sup> Q. Gao, E. Li, and A.X. Wang, "Ultra-compact and broadband

- electro-absorption modulator using an epsilon-near-zero conductive oxide," Photonics Res. **6**(4), 277–281 (2018).
- <sup>16</sup> V.J. Sorger, N.D. Lanzillotti-Kimura, R.-M. Ma, and X. Zhang, "Ultra-compact silicon nanophotonic modulator with broadband response," Nanophotonics **1**(1), 17–22 (2012).
- <sup>17</sup> R. Amin, R. Maiti, Y. Gui, C. Suer, M. Miscuglio, E. Heidari, R.T. Chen, H. Dalir, and V.J. Sorger, "Sub-wavelength GHz-fast broadband ITO Mach-Zehnder modulator on silicon photonics," Optica **7**(4), 333–335 (2020).
- <sup>18</sup> A. Melikyan, N. Lindenmann, S. Walheim, P.M. Leufke, S. Ulrich, J. Ye, P. Vincze, H. Hahn, T. Schimmel, C. Koos, W. Freude, and J. Leuthold, "Surface plasmon polariton absorption modulator," Opt. Express 19(9), 8855–8869 (2011).
- <sup>19</sup> M.G. Wood, S. Campione, S. Parameswaran, T.S. Luk, J.R. Wendt, D.K. Serkland, and G.A. Keeler, "Gigahertz speed operation of epsilon-near-zero silicon photonic modulators," Optica **5**(3), 233–236 (2018).
- <sup>20</sup> E. Li, Q. Gao, R.T. Chen, and A.X. Wang, "Ultracompact Silicon-Conductive Oxide Nanocavity Modulator with 0.02 Lambda-Cubic Active Volume," Nano Lett. **18**(2), 1075–1081 (2018).
- <sup>21</sup> E. Li, B.A. Nia, B. Zhou, and A.X. Wang, "Transparent conductive oxide-gated silicon microring with extreme resonance wavelength tunability," Photonics Res. **7**(4), 473–477 (2019).
- <sup>22</sup> P.R. West, S. Ishii, G. V Naik, N.K. Emani, V.M. Shalaev, and A. Boltasseva, "Searching for better plasmonic materials," Laser \& Photonics Rev. 4(6), 795–808 (2010).
- <sup>23</sup> A. Boltasseva, and H.A. Atwater, "Low-Loss Plasmonic Metamaterials," Science (80-.). **331**(6015), 290–291 (2011).
- <sup>24</sup> Z. Ma, Z. Li, K. Liu, C. Ye, and V.J. Sorger, "Indium-Tin-Oxide for High-performance Electro-optic Modulation," Nanophotonics **4**(2), 198–213 (2015).
- <sup>25</sup> V.E. Babicheva, A. Boltasseva, and A. V Lavrinenko, "Transparent conducting oxides for electro-optical plasmonic modulators," Nanophotonics **4**(2), 165–185 (2015).
- <sup>26</sup> W. Jaffray, S. Saha, V.M. Shalaev, A. Boltasseva, and M. Ferrera, "Transparent conducting oxides: from all-dielectric plasmonics to a new paradigm in integrated photonics," Adv. Opt. Photon. **14**(2), 148–208 (2022).
- <sup>27</sup> I. Liberal, and N. Engheta, "Near-zero refractive index photonics," Nat. Photonics **11**(3), 149–158 (2017).
- <sup>28</sup> J. Wu, Z.T. Xie, Y. Sha, H.Y. Fu, and Q. Li, "Epsilon-near-zero photonics: infinite potentials," Photon. Res. **9**(8), 1616–1644 (2021).
- <sup>29</sup> X. Niu, X. Hu, S. Chu, and Q. Gong, "Epsilon-Near-Zero Photonics: A New Platform for Integrated Devices," Adv. Opt. Mater. **6**(10), 1701292 (2018).
- <sup>30</sup> S. Campione, M.G. Wood, D.K. Serkland, S. Parameswaran, J. Ihlefeld, T.S. Luk, J.R. Wendt, K.M. Geib, and G.A. Keeler, "Submicrometer Epsilon-Near-Zero Electroabsorption Modulators Enabled by High-Mobility Cadmium Oxide," IEEE Photonics J. 9(4), 1–7 (2017).
- <sup>31</sup> A.P. Vasudev, J.-H. Kang, J. Park, X. Liu, and M.L. Brongersma, "Electro-optical modulation of a silicon waveguide with an ''epsilonnear-zero'' material," Opt. Express **21**(22), 26387–26397 (2013).
- <sup>32</sup> J. Baek, J.-B. You, and K. Yu, "Free-carrier electro-refraction modulation based on a silicon slot waveguide with ITO.," Opt. Express **23**(12), 15863–15876 (2015).
- <sup>33</sup> S. Zhu, G.Q. Lo, and D.L. Kwong, "Design of an ultra-compact electro-absorption modulator comprised of a deposited TiN/HfO2/ITO/Cu stack for CMOS backend integration," Opt. Express **22**(15), 17930–17947 (2014).
- <sup>34</sup> Z. Lu, W. Zhao, and K. Shi, "Ultracompact Electroabsorption Modulators Based on Tunable Epsilon-Near-Zero-Slot Waveguides," IEEE Photonics J. **4**(3), 735–740 (2012).
- <sup>35</sup> A.O. Zaki, K. Kirah, and M.A. Swillam, "Hybrid plasmonic electrooptical modulator," Appl. Phys. A **122**(4), 473 (2016).
- <sup>36</sup> C. Huang, R.J. Lamond, S.K. Pickus, Z.R. Li, and V.J. Sorger, "A

- Sub-λ-Size Modulator Beyond the Efficiency-Loss Limit," IEEE Photonics J. **5**(4), 2202411 (2013).
- <sup>37</sup> U. Koch, C. Hoessbacher, J. Niegemann, C. Hafner, and J. Leuthold, "Digital plasmonic absorption modulator exploiting epsilon-near-zero in transparent conducting oxides," IEEE Photonics J. **8**(1), 1–13 (2016).
- <sup>38</sup> A. V. Krasavin, and A. V. Zayats, "Photonic signal processing on electronic scales: Electro-optical field-effect nanoplasmonic modulator," Phys. Rev. Lett. **109**(5), 053901 (2012).
- <sup>39</sup> G. Sinatkas, A. Pitilakis, D.C. Zografopoulos, R. Beccherelli, and E.E. Kriezis, "Transparent conducting oxide electro-optic modulators on silicon platforms: A comprehensive study based on the drift-diffusion semiconductor model," J. Appl. Phys. **121**(2), 23109 (2017). <sup>40</sup> Q. Gao, E. Li, and A.X. Wang, "Comparative analysis of transparent conductive oxide electro-absorption modulators \[Invited\]," Opt. Mater. Express **8**(9), 2850–2862 (2018).
- <sup>41</sup> W.-C. Hsu, B. Zhou, and A.X. Wang, "MOS Capacitor-Driven Silicon Modulators: A Mini Review and Comparative Analysis of Modulation Efficiency and Optical Loss," IEEE J. Sel. Top. Quantum Electron. **28**(3), 1–11 (2022).
- <sup>42</sup> N. Kinsey, C. DeVault, A. Boltasseva, and V.M. Shalaev, "Nearzero-index materials for photonics," Nat. Rev. Mater. **4**(12), 742–760 (2019).
- <sup>43</sup> I. Liberal, and N. Engheta, "The rise of near-zero-index technologies," Science (80-.). **358**(6370), 1540–1541 (2017).
- <sup>44</sup> O. Reshef, I. De Leon, M.Z. Alam, and R.W. Boyd, "Nonlinear optical effects in epsilon-near-zero media," Nat. Rev. Mater. **4**(8), 535–551 (2019).
- <sup>45</sup> G. Briere, B. Cluzel, and O. Demichel, "Improving the transmittance of an epsilon-near-zero-based wavefront shaper," Opt. Lett. **41**(19), 4542–4545 (2016).
- <sup>46</sup> X.-T. He, Z.-Z. Huang, M.-L. Chang, S.-Z. Xu, F.-L. Zhao, S.-Z. Deng, J.-C. She, and J.-W. Dong, "Realization of Zero-Refractive-Index Lens with Ultralow Spherical Aberration," ACS Photonics **3**(12), 2262–2267 (2016).
- <sup>47</sup> L. Caspani, R.P.M. Kaipurath, M. Clerici, M. Ferrera, T. Roger, J. Kim, N. Kinsey, M. Pietrzyk, A. Di Falco, V.M. Shalaev, A. Boltasseva, and D. Faccio, "Enhanced Nonlinear Refractive Index in ε-Near-Zero Materials," Phys. Rev. Lett. **116**(23), 233901 (2016).
- <sup>48</sup> A. Capretti, Y. Wang, N. Engheta, and L.D. Negro, "Enhanced third-harmonic generation in Si-compatible epsilon-near-zero indium tin oxide nanolayers," Opt. Lett. **40**(7), 1500–1503 (2015).
- <sup>49</sup> A. Capretti, Y. Wang, N. Engheta, and L. Dal Negro, "Comparative Study of Second-Harmonic Generation from Epsilon-Near-Zero Indium Tin Oxide and Titanium Nitride Nanolayers Excited in the Near-Infrared Spectral Range," ACS Photonics **2**(11), 1584–1591 (2015).
- <sup>50</sup> R. Amin, R. Maiti, C. Carfano, Z. Ma, M.H. Tahersima, Y. Lilach, D. Ratnayake, H. Dalir, and V.J. Sorger, "0.52 v mm ITO-based Mach-Zehnder modulator in silicon photonics," APL Photonics 3(12), 126104 (2018).
- <sup>51</sup> J. Park, J.-H. Kang, X. Liu, and M.L. Brongersma, "Electrically Tunable Epsilon-Near-Zero (ENZ) Metafilm Absorbers," Sci. Rep. **5**(1), 15754 (2015).
- <sup>52</sup> Y. Yang, K. Kelley, E. Sachet, S. Campione, T.S. Luk, J.-P. Maria, M.B. Sinclair, and I. Brener, "Femtosecond optical polarization switching using a cadmium oxide-based perfect absorber," Nat. Photonics 11(6), 390–395 (2017).
- <sup>53</sup> E. Li, Q. Gao, S. Liverman, and A.X. Wang, "One-volt silicon photonic crystal nanocavity modulator with indium oxide gate," Opt. Lett. **43**(18), 4429–4432 (2018).
- <sup>54</sup> E. Li, B. Zhou, Y. Bo, and A.X. Wang, "High-Speed Femto-Joule per Bit Silicon-Conductive Oxide Nanocavity Modulator," J. Light. Technol. **39**(1), 178–185 (2021).
- <sup>55</sup> W.-C. Hsu, E. Li, B. Zhou, and A.X. Wang, "Characterization of field-effect mobility at optical frequency by microring resonators,"

- Photonics Res. 9(4), 615-621 (2021).
- <sup>56</sup> W.-C. Hsu, C. Zhen, and A.X. Wang, "Electrically Tunable High-Quality Factor Silicon Microring Resonator Gated by High Mobility Conductive Oxide," ACS Photonics **8**(7), 1933–1936 (2021).
- <sup>57</sup> W.-C. Hsu, N. Nujhat, B. Kupp, J.F. Conley, and A.X. Wang, "Onchip wavelength division multiplexing filters using extremely efficient gate-driven silicon microring resonator array," Sci. Rep. **13**(1), 5269 (2023).
- <sup>58</sup> E. Li, and A.X. Wang, "Theoretical Analysis of Energy Efficiency and Bandwidth Limit of Silicon Photonic Modulators," J. Light. Technol. **37**(23), 5801–5813 (2019).
- <sup>59</sup> Y. Gui, M. Miscuglio, Z. Ma, M.H. Tahersima, S. Sun, R. Amin, H. Dalir, and V.J. Sorger, "Towards integrated metatronics: a holistic approach on precise optical and electrical properties of Indium Tin Oxide," Sci. Rep. **9**(1), 11279 (2019).
- <sup>60</sup> F. Fuchs, and F. Bechstedt, "Indium-oxide polymorphs from first principles: Quasiparticle electronic states," Phys. Rev. B 77(15), 155107 (2008).
- <sup>61</sup> T. Koida, Y. Ueno, and H. Shibata, "In2O3-Based Transparent Conducting Oxide Films with High Electron Mobility Fabricated at Low Process Temperatures," Phys. Status Solidi **215**(7), 1700506 (2018).
- <sup>62</sup> A. Chaoumead, H.-D. Park, B.-H. Joo, D.-J. Kwak, M.-W. Park, and Y.-M. Sung, "Structural and Electrical Properties of Titanium-Doped Indium Oxide Films Deposited by RF Sputtering," Energy Procedia **34**, 572–581 (2013).
- <sup>63</sup> E. Sachet, C.T. Shelton, J.S. Harris, B.E. Gaddy, D.L. Irving, S. Curtarolo, B.F. Donovan, P.E. Hopkins, P.A. Sharma, A.L. Sharma, J. Ihlefeld, S. Franzen, and J.-P. Maria, "Dysprosium-doped cadmium oxide as a gateway material for mid-infrared plasmonics," Nature Materials 14(4), 414–420 (2015).
- <sup>64</sup> B. Zhou, E. Li, Y. Bo, and A.X. Wang, "High-Speed Plasmonic-Silicon Modulator Driven by Epsilon-Near-zero Conductive Oxide," J. Light. Technol. 38(13), 3338–3345 (2020).
- <sup>65</sup> C. Hoessbacher, Y. Fedoryshyn, A. Emboras, A. Melikyan, M. Kohl, D. Hillerkuss, C. Hafner, and J. Leuthold, "The plasmonic memristor: a latching optical switch," Optica **1**(4), 198–202 (2014).
- <sup>66</sup> Y. Huang, J. Zheng, B. Pan, L. Song, K.-A. Chen, Z. Yu, H. Ye, and D. Dai, "High-bandwidth Si/In2O3 hybrid plasmonic waveguide modulator," APL Photonics 7(5), 51301 (2022).
- <sup>67</sup> W.-C. Hsu, N. Nujhat, B. Kupp, J.F. Conley, H. Rong, R. Kumar, and A.X. Wang, "Sub-Volt High-Speed Silicon MOSCAP Microring Modulator Driven by High Mobility Conductive Oxide," (2023). Available: <a href="https://doi.org/10.48550/arXiv.2308.16255">https://doi.org/10.48550/arXiv.2308.16255</a>.
- <sup>68</sup> D.S. Zemtsov, I.A. Pshenichnyuk, S.S. Kosolobov, A.K. Zemtsova, D.M. Zhigunov, A.S. Smirnov, K.N. Garbuzov, and V.P. Drachev, "Plasmon-Assisted Si-ITO Integrated Electro-Optical Rib-Shape Modulator," J. Light. Technol., 1–5 (2023).
- <sup>69</sup> M.G. Wood, P.S. Finnegan, K.M. Musick, W.M. Mook, C.D. Nordquist, A.J. Grine, and D.K. Serkland, "Epsilon-Near-Zero Modulators Integrated on Si3N4 Waveguides for Operation Shorter than 1μm," Frontiers in Optics, JTu4A.79 (2023).